Electron Transport in Amorphous Metal–Carbon Nanocomposite Films

A. D. Bozhko[a], E. A. Kataeva[b], T. Takagi[c], M. G. Mikheev[a], and M. B. Guseva[b]

[a] *Department of Low Temperature Physics and Superconductivity, Faculty of Physics, Moscow State University,
Leninskie gory, Moscow, 119992 Russia*

e-mail: bozhko@mig.phys.msu.ru

[b] *Department of Physical Electronics, Faculty of Physics, Moscow State University,
Leninskie gory, Moscow, 119992 Russia*

[c] *Institute of Fluid Science, Tohoku University, Sendai, Japan*

Received February 17, 2006

Abstract—The electrical conductivity of amorphous silicon- and oxygen-containing W-, Nb-, and Cr-carbon nanocomposite films is studied. It is revealed that, at a metal concentration of 10–40 at. % and in the temperature range 80–400 K, the electrical conductivity of the films is a power function of temperature. In terms of inelastic electron tunneling, the average number of localized states in the intercluster potential barriers is calculated as a function of the metal concentration.

INTRODUCTION

Solid films of amorphous carbon a-C:H, ta-C, and ta-C:H are widely used as protective coatings of various types [1]. The field of possible application of these materials can be extended considerably owing to variability of their properties upon doping by various elements. The most frequently used dopants are silicon [2], nitrogen [3], and various metals [4]. Of most interest is the addition of metals to the films during their deposition. Among other changes, this increases the conductivity of initially dielectric films by several orders of magnitude, i.e., up to the values typical of amorphous metals [4].

The metal–carbon nanocomposite films are interesting not only in their new practical applications. Of fundamental interest are the conduction mechanisms under conditions of strong disorder typical of amorphous carbon.

Commonly used dopants are the IV–VI transient refractory metals. The metal–carbon composites based on these metals have a high thermal stability [5]. In this study, we investigate the electron transport and structure of the carbon phase in the metal–carbon–silicon nanocomposite films containing W, Nb and Cr as their concentrations vary over a wide range from 10 to 40 at. %.

EXPERIMENTAL

Metal–carbon nanocomposite films were grown to a thickness of 0.5–1.0 μm on substrates of polished glass ceramic by a combination of two processes: the decomposition of vapors of an organosilicon polymer, polyphenyl methylsiloxane $(CH_3)_3SiO(CH_3C_6H_5SiO)_3Si(CH_3)_3$, in stimulated dc discharge plasma and the dc magnetron sputtering of the corresponding metal (W, Nb, or Cr) target. The deposition energy was controlled by a high-frequency potential of 1.76 MHz applied to a metal substrate holder. The film deposition process was described in detail in [6].

The film conductivity was measured by the dc four-terminal method in the temperature range 80–400 K in a blow-through cryostat. The samples for the conductivity measurements in standard geometry were subjected to etching in RF-discharge plasma (13.56 MHz) in argon using a mechanical mask. To decrease the contact resistance, a golden sublayer was deposited on the contact pads. The contacts to the samples were prepared from silver paste and then heat-treated at 180°C for 10 min in argon.

The carbon phase structure was investigated by means of Raman spectroscopy performed on a Jobin Yvon LabRAM HR-800 spectrometer using the 632.8 nm line of the He-Ne laser in the range 800–1800 cm^{-1}.

The metal phase structure was studied by the electron diffraction method on a JSEM-100C transmission electron microscope.

The elemental composition of the films was determined by electron-probe microanalysis on a JEOL JXA-8200 spectrometer.

RESULTS AND DISCUSSION

The conductivity temperature curves $\sigma(T)$ look similar for all types of films studied. They are characterized
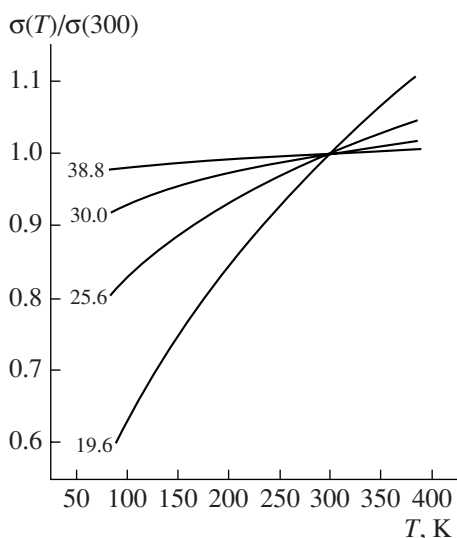
Fig. 1. Temperature dependences of conductivity normalized to the value at room temperature $\sigma(300)$ for the Cr-carbon nanocomposite films. The numbers are Cr concentrations.

by a decrease in the conductivity with decreasing temperature throughout the metal concentration range studied and are closely approximated by the power function,

$$\sigma = \sigma_0 + aT^p, \qquad (1)$$

where σ_0, a, and p are the parameters depending on the metal type and concentration. Figure 1 presents typical temperature dependences $\sigma(T)$ of the conductivity nor-

malized to the conductivity value at room temperature $\sigma(300)$ for the Cr-containing films.
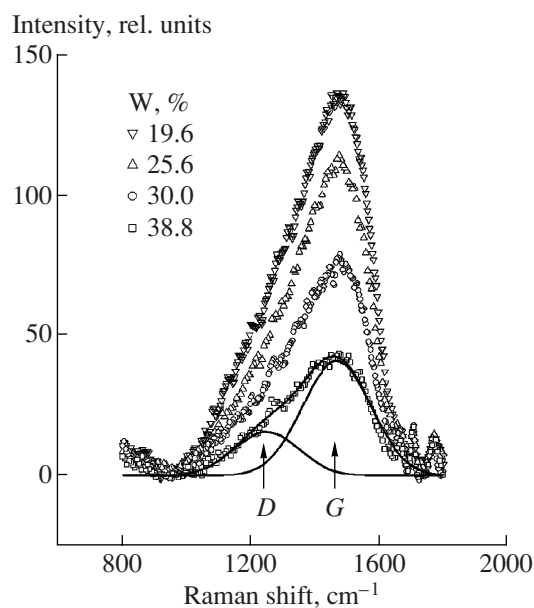
The Raman spectra of the films are also very similar in appearance for the three types of films studied. They display an asymmetric peak at about 1450–1500 cm⁻¹, which is typical of amorphous carbon. The peak amplitude shows a strong descending dependence on the metal concentration in the films. Conventionally for amorphous carbon films, this peak can be decomposed into two Gaussian peaks called the D and G peaks located at 1300–1400 cm⁻¹ and 1450–1600 cm⁻¹, respectively. The presence of the D peak in the Raman spectrum of amorphous carbon is due to the A_{1g} breathing modes of six-fold aromatic rings. The G peak is related to the E_{2g} compression–tension vibrations of the carbon bonds [1].

Figure 2 presents the Raman spectra of the W-containing films and their approximation by two Gaussian peaks.

The character of electron diffraction at the metal–carbon nanocomposite films points to a highly dispersed, close to amorphous structure of the metal phase. Figure 3 shows the electron diffraction profile minus the Gaussian background and the inset presents a fragment of the diffraction pattern for the tungsten–carbon nanocomposites. Calculated from the diffraction profiles, the average size of the regions of metal phase coherent scattering ranges 1–2 nm in the studied films and tends to increase with increasing metal concentration. The size of conducting inclusions may differ from the value above because of the transition layer that arises at the metal granule boundaries as a result of the formation of chemical bonds between the metals and the matrix elements.

The conductivity–temperature dependence of the metal–carbon nanocomposite films may be considered in terms of the model of inelastic electron tunneling in

Fig. 2. Raman spectra of the W-carbon nanocomposite films. Gaussian peaks D and G are shown within the spectrum of films with 19.6 at. %.
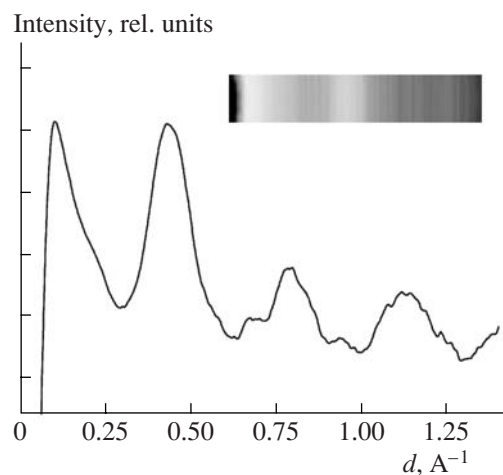
Fig. 3. Electron diffraction profile of the W-carbon nanocomposite films. Inset shows a fragment of the electron diffraction pattern.

thin dielectric films. As shown in [7], the presence of n localized states in the potential barrier between metal contacts leads to the power dependence

$$\sigma_n \sim e^2 \left(\frac{\Lambda^2 E_0^2}{\rho c^5} \right)^{\frac{n-1}{n+1}}$$

$$\times g^n n^{2n} a^{2n-1} d^{n-1} E_0^{\frac{2}{n+1}} T^{n - \frac{2}{n+1}} \exp\left(-\frac{2d}{a(n+1)} \right),$$

(2)

where d is the distance between electrodes, Λ is the deformation potential constant, ρ is the material density, c is the speed of sound, g is the density of localized states, a is the localization radius, e is the electron charge, and E_0 is the depth of the localized states in the barrier region.

Assuming electron tunneling between the metal granules or between the clusters of such granules to be the main mechanism of electron transport in amorphous metal-containing silicon–carbon nanocomposites, the model of inelastic electron tunneling relates the average number of states $\langle n \rangle$ localized in the carbon matrix in the potential barriers between the metal clusters to the power index p in expression (1),

$$\langle n \rangle = \frac{1}{2}\left(p - 1 + (p^2 + 2p + 9)^{\frac{1}{2}} \right).$$

(3)

The dependences of $\langle n \rangle$ on the metal concentration in the silicon–carbon nanocomposite films containing W, Nb, and Cr are presented in Fig. 4. It is seen that the dependences for the W- and Nb-containing films have much in common. At a low content of the metals, $\langle n \rangle$ decreases with concentration from 2.5 to 1.3 and from 1.8 to 1.2 in the W- and Nb-containing films, respectively. As the concentration of metals exceeds 22–23 at. %, $\langle n \rangle$ starts to grow and reaches 1.4–1.5 at 40 at. % of W or Nb. In contrast, the average number of localized states in the Cr-containing films only slightly increases with the metal concentration and remains in the vicinity of 1.2.

In terms of the model discussed, the concentration behavior of $\langle n \rangle$ can be attributed to competition between the two main mechanisms. One mechanism is a decrease in the distance between metal clusters with an increase in the metal concentration. The other mechanism relates to the possible dependence of the density of defects in the carbon–silicon matrix on the metal concentration. Obviously, as a result of the competition between these two mechanisms, the number of states localized in the intercluster potential barriers may either decrease or increase with an increase in the metal concentration.

As the metal content grows from 10 to 40 at. %, the Si concentration in the films smoothly decreases in the ranges 19–14, 20–18, and 18–15 at. % for the W-, Nb-, and Cr-containing films, respectively. The oxygen concentration behaves similarly. It decreases from 16 to
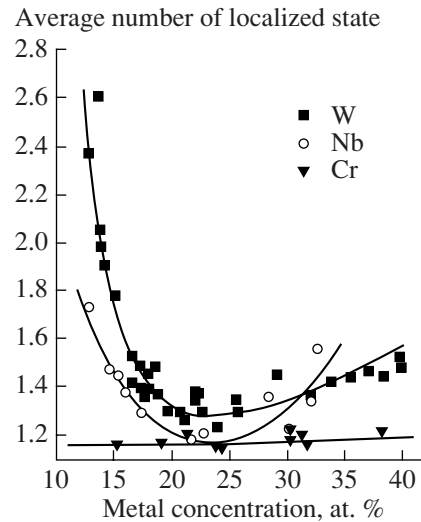
Fig. 4. Average number of localized states in the intercluster potential barriers vs. the metal concentrations in the metal–carbon nanocomposite films.

12 at. % in the W- and Nb-containing films and from 10 to 2 at. % in the Cr-containing films. At the metal concentrations 20–25 at. %, nothing unusual in the behavior of the silicon and oxygen concentrations is detected. This allows one to suppose that the observed increase in the defect density cannot be attributed to a decrease in the oxygen and silicon concentrations in the films.

Figure 5 presents the ratio of the Raman D and G peak amplitudes as a function of the metal concentration for all the types of the films studied. Similar to the case with the conductivity curves, two types of the dependences can be distinguished. In the W- and Nb-containing silicon–carbon nanocomposite films, the $I(D)/I(G)$ ratio sharply increases from 0.9 to 1.9 in the concentration range 20–25 at. %. In contrast, the Cr-containing films are characterized by a constant $I(D)/I(G)$ ratio close to 0.9.

It was suggested in [8] that an increase in the D and G peak ratio in the amorphous carbon films can be explained by the ordering of the carbon sp^2 phase. In accordance with the three-stage model proposed in [8], this increase in the $I(D)/I(G)$ ratio may occur owing to the integration of the carbon sp^2 states into aromatic graphite-like clusters. In terms of this model, an increase in the W and Nb concentrations above 22–25 at. % in the amorphous silicon–carbon films may lead to an increase in the characteristic size of graphite cluster. An increase in $\langle n \rangle$ observed in the W- and Nb-containing films over the same range of the metal concentration points to a relation between the localized states, which influence the film conductivity, and the carbon sp^2 clusters. It is not improbable that the defects involved in the electron tunneling are the localized states at the sp^2 cluster boundaries [9].
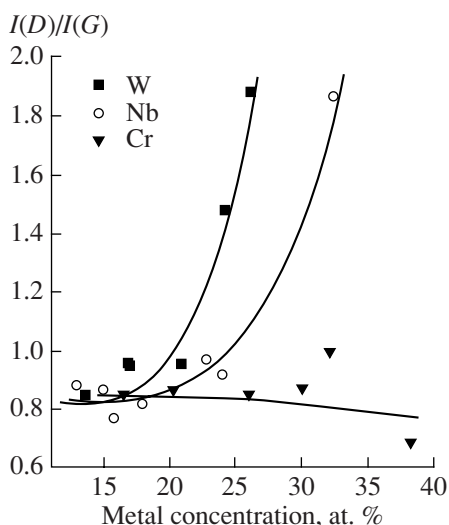
Fig. 5. Ratio of the Raman peak amplitudes $I(D)/I(G)$ vs. the metal concentration in the W-, Nb-, and Cr-containing nanocomposite films.

However, the growth of the sp^2 clusters may result also in the compacting of the current-carrying skeleton of an infinite conducting cluster, so that the distances in the tunnel gaps grow with an increase in the W and Nb concentrations. This may also lead to the observed increase in the average number of localized states in the barriers.

An increase in the Cr concentration in the carbon–silicon matrix, on the contrary, leads to only a slight variation of $\langle n \rangle$ and characteristic size of the sp^2 clusters. A weak dependence of $\langle n \rangle$ on the Cr concentration may be explained by the fact that the increased transparency of the intercluster potential barriers is mainly due to the states localized at the Cr granule boundaries. In this case, the average number of localized states in the lines of current depends neither on the distance between the Cr clusters nor on the metal concentration.

The main distinction of chromium from niobium and tungsten is its ability to form a compound carbide of the $Cr_{23}C_6$ type [10], which is probably responsible for the localized states specified. Moreover, the presence of $Cr_{23}C_6$ may also preclude the sp^2 cluster growing with an increase in the Cr concentration.

CONCLUSIONS

Conductivity of the amorphous silicon–carbon nanocomposite films containing W, Nb, and Cr was studied as a function of an increasing metal concentra-tion. The film conductivity was shown to obey the power law in a wide range of temperatures (80–400 K) and metal concentrations (10–40 at. %). The charge transport in the metal–carbon nanocomposite films is adequately described in terms of the model of inelastic electron tunneling between the metal clusters via the localized states in the carbon–silicon matrix. The calculated average of the number of localized states $\langle n \rangle$ in the intercluster potential barriers is a nonmonotonic function of the metal concentration in the W- and Nb-containing films and is close to a constant value in the Cr-containing films.

Finally, the behavior of the carbon phase structure with an increase in the metal concentration was investigated by means of Raman spectroscopy. In the carbon films containing W and Nb, the sp^2 clusters grew in size as the metal concentration exceeded 22–25%. The cluster growth was used to explain the increase in the density of localized states in the intercluster space observed for the W- and Nb-containing films. The fact that the density of localized states is almost independent of the Cr concentration in the Cr-containing films is explained by assigning the major part of the conductivity to the defects present at the Cr cluster boundaries.

REFERENCES

1. J. Robertson, Mater. Sci. Eng., R. **37**, 129 (2002).
2. C. De Martino, G. Fusco, G. Mino, et al., Diamond Relat. Mater. **6**, 559 (1977).
3. J. Koskinen, J.-P. Hirvonen, J. Levosko, and P. Torri, Diamond Relat. Mater. **6**, 669 (1996).
4. H. Dimigen, H. Hübsch, and R. Memmig, Appl. Phys. Lett. **50**, 1056 (1987).
5. B. F. Dorfman, Thin Solid Films **330**, 76 (1998).
6. B. F. Dorfman, in *Handbook of Surfaces and Interfaces of Materials*, Ed. By H. S. Nalwa, Vol. 1: *Surfaces and Interface Phenomena* (Academic, New York, 2001).
7. L. I. Glazman and K. A. Matveev, Zh. Éksp. Teor. Fiz. **94**, 332 (1988) [Sov. Phys. JETP **67**, 1276 (1988)].
8. A. C. Ferrari and J. Robertson, Phys. Rev. B **61**, 14095 (2000).
9. D. Dasgupta, F. Demichelis, and A. Tagliaferro, Phil. Mag. B **63**, 1255 (1991).
10. A. F. Wells, *Structural Inorganic Chemistry* (Clarendon, Oxford, England, 1984; Mir, Moscow, 1988).